

Cherenkov Radiation from a Hollow Conical Targets: Off-Axis Charge Motion

Andrey V. Tyukhtin* and Sergey N. Galyamin

Saint Petersburg State University, 7/9 Universitetskaya nab., St. Petersburg, 199034 Russia

Viktor V. Vorobev

Technical University of Munich, Germany, Department of Informatics

(Dated: May 5, 2021)

Cherenkov radiation (CR) generated by a charge moving through a hollow conical target made of dielectric material is analyzed. We consider two cases: the charge moves from the base of the cone to its top (“straight” cone) or from the top to the base (“inverted” cone). Unlike previous works, a nonzero shift of the charge trajectory from the symmetry axis is taken into account which leads to generation of nonsymmetrical radiation. The most interesting effect is the phenomenon of “Cherenkov spotlight” which has been reported earlier for axially symmetrical problems. This effect allows essential enhancement of the CR intensity in the far-field region by proper selection of the target’s parameters and charge velocity. Here we describe the influence of charge shift on CR far-field patterns paying the main attention to the “Cherenkov spotlight” regime. Influence of variation of the charge speed on this phenomenon is also investigated.

I. INTRODUCTION

Radiation of charged particles moving in presence of dielectric objects (“targets”) of complicated form is of interests for various applications [1–5]. As an example, one can mention a new method of bunch diagnostics which requires calculation of Cherenkov radiation outside dielectric object [2]. Typically, the size of the target is much larger than the wavelengths under consideration. On the one hand, this fact complicates considerably computer simulations because they require very large amount of resources and time. On the other hand, this fact gives us an obvious small parameter of the problem and allows developing approximate methods of analysis.

Previously, we have developed two methods for solution of such problems which can be named as “ray-optic method” and “aperture method”. Both these methods are valid for objects which are much larger than the wavelengths under consideration. The basis of the methods and solutions of different problems with use of them are describes in series of our papers [6–18]. We do not repeat here the main steps of the methods. Note only that the aperture method is more general than the ray optics one (the last one can not describe different diffraction effects and requires additional limitation on the observation point place). Therefore we will use here the aperture technique.

It should be emphasized that this method has been tested for various objects, in particular, for a dielectric cone and a ball with vacuum channel (in the cases of axially symmetric problems). The testing was conducted by comparison with COMSOL simulation. As a result, it has been shown (as expected) that the aperture method gives an accuracy of the order of the ratio of the considered wavelength to the size of the object (at least in the

regions of the maximal field magnitudes). This conclusion is especially important in the context of this article, because we are primarily interested in the region of the main maximum of the angle diagram.

Earlier, we considered two problems with a dielectric cone having a vacuum channel under condition that the charge trajectory coincides with the symmetry axis of the cone [13, 17]. One problem assumes the motion of the charge from the cone base to the cone top (“straight” cone), and the other deals with the charge movement from the top to the base (“inverted” cone). In both problems, the most interesting phenomenon is an effect named by us the “Cherenkov spotlight”. This effect allows essential increasing the CR intensity in the far-field (Fraunhofer) area by proper selection of the target’s parameters and charge velocity. The effect takes place if the refracted waves in the ray optics area are parallel to the symmetry axis. In this case the maximal radiation in the Fraunhofer area is observed at some small (but nonzero!) angle with respect to this axis. This radiation is much more intensive than one the radiation in other situations.

We analyzed earlier only the axially symmetrical problems where the charge moves on the symmetry axis. It is important to establish how sensitive the spotlight effect is with respect to the position of the charge trajectory in the channel cross section. Here we study the case when the charge moves parallel to the cone symmetry axis but it’s trajectory is shifted from it. We consider both the “straight” cone and the “inverted” one. These problems are essentially more complex than the previous ones [13, 17] because of a cylindrical symmetry is absent. We pay the main attention to analysis of radiation in the far-field zone, especially to the Cherenkov spotlight effect.

* a.tyukhtin@spbu.ru

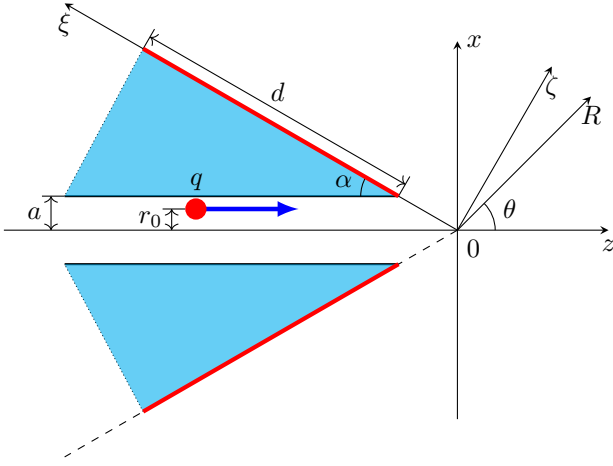


Figure 1. The cone cross-section.

II. THE CASE OF THE “STRAIGHT” CONE

A. The field on the aperture

We analyze radiation of a charge moving along the axis of the cylindrical channel with radius a in a conical object (Fig. 1) made of dielectric material with permittivity ε , permeability $\mu = 1$ and negligible conductivity. In this section we assume that the charge moves from the target base to its top. In this situation the actual form of the lateral border of the target is not principal (dotted line in Fig. 1), only the aperture with size d illuminated by CR is important (red lines in Fig. 1). The target sizes are supposed to be much larger than wavelengths under consideration: $d \gg \lambda$. The coordinate system origin is at the cone apex, and the z -axis is the symmetry axis of the target.

The point charge q moves with constant velocity $\vec{v} = c\beta\vec{e}_z$ parallel to z -axis along the straight trajectory shifted by r_0 along x -axis. The charge density is $\rho = q\delta(x - r_0)\delta(y)\delta(z - c\beta t)$, where δ is a Dirac delta-function. It is assumed that the charge velocity exceeds the “Cherenkov threshold”, i.e. $\beta > 1/n$, where $n = \sqrt{\varepsilon}$ is a refractive index of the target material. Therefore, CR is generated in the cone material.

We will use here the same notations as in the paper of Tyukhtin et al. [13]. The “main” wave is the wave which causes the “Cherenkov spotlight” effect. The way of this wave is the same as in the axially symmetrical case $r_0 = 0$ (see Fig. 2 in [13]). The CR wave generated by a moving charge in the bulk of the target incidents

the inner surface of the aperture at the angle

$$\theta_i = \pi/2 - \alpha - \theta_p, \quad \theta_p = \arccos[1/(n\beta)],$$

and then refracted at the angle

$$\theta_t = \arcsin(1/(n\beta))$$

with respect to the boundary normal \vec{e}_ζ (see Fig. 2 in [13]).

Due to the asymmetry caused by the charge trajectory shift, CR of both polarizations is generated. “Parallel” polarization (\parallel) contains components E_z , E_r and H_φ . Corresponding Fresnel transmission coefficient (for the transmission at the cone generatrix) is

$$T_{\parallel} = \frac{2 \cos \theta_i}{\cos \theta_i + \sqrt{\varepsilon} \cos \theta_t}. \quad (1)$$

“Orthogonal” polarization (\perp) contains components H_z , H_ρ and E_φ . Corresponding Fresnel coefficient is

$$T_{\perp} = \frac{2\sqrt{\varepsilon} \cos \theta_i}{\sqrt{\varepsilon} \cos \theta_i + \cos \theta_t}. \quad (2)$$

Based on results of our previous papers [14–16] we can write the CR field before the refraction at the cone generatrix surface. For \parallel polarization, the Fourier-transform of the azimuthal magnetic component at the distance $r \gg \lambda$ is

$$H_\varphi^i(r, \varphi, z) = \frac{-q\omega}{\pi v^2 \gamma^2} \sqrt{\frac{2}{\pi r s}} \exp[i\Phi_i(r, z)] \times \frac{ik}{s} \left\{ -\varepsilon I_0(r_0\sigma) \tilde{A}_0^{(E2)} + 2 \sum_{\nu=1}^{\infty} I_\nu(r_0\sigma) e^{\frac{i\pi(1-\nu)}{2}} \times \cos(\nu\varphi) i\varepsilon \tilde{A}_\nu^{(E2)} \right\}. \quad (3)$$

For \perp polarization, the Fourier-transform of the azimuthal electric component is

$$E_\varphi^i(r, \varphi, z) = \frac{q\omega}{\pi v^2 \gamma^2} \sqrt{\frac{2}{\pi r s}} \exp[i\Phi_i(r, z)] \times \frac{ik}{s} 2 \sum_{\nu=1}^{\infty} I_\nu(r_0\sigma) e^{\frac{i\pi(1-\nu)}{2}} \sin(\nu\varphi) \tilde{A}_\nu^{(H2)} \quad (4)$$

Here we introduce the following notations:

$$\tilde{A}_0^{(E1)} = -\frac{\sigma^2 s \varepsilon H'_0 K_0 + \sigma s^2 K'_0 H_0}{\sigma^2 s \varepsilon H'_0 I_0 + \sigma s^2 I'_0 H_0},$$

$$\tilde{A}_\nu^{(E1)} = \frac{1}{\Delta_\nu H_\nu^2} \left\{ -[\nu(\beta a)^{-1} I_\nu(\sigma^2 + s^2)]^2 H_\nu^2 K_\nu I_\nu^{-1} + [\sigma^2 s \mu H'_\nu I_\nu + s^2 \sigma I'_\nu H_\nu] [\sigma^2 s \varepsilon H'_\nu K_\nu + s^2 \sigma K'_\nu H_\nu] \right\}, \quad (5)$$

$$\tilde{A}_\nu^{(H1)} = \frac{\nu I_\nu(\sigma^2 + s^2)}{i\beta a \Delta_\nu H_\nu} \{ [\sigma^2 s \varepsilon H'_\nu K_\nu + s^2 \sigma K'_\nu H_\nu] - K_\nu I_\nu^{-1} [\sigma^2 s \varepsilon H'_\nu I_\nu + s^2 \sigma I'_\nu H_\nu] \}, \quad (6)$$

$$\Delta_\nu = [\nu(\beta a)^{-1} I_\nu(\sigma^2 + s^2)]^2 - \frac{[\sigma^2 s \varepsilon H'_\nu I_\nu + s^2 \sigma I'_\nu H_\nu][\sigma^2 s \mu H'_\nu I_\nu + s^2 \sigma I'_\nu H_\nu]}{H_\nu^2}, \quad (7)$$

where

$$k = \omega/c, \quad s = k\sqrt{\varepsilon\beta^2 - 1}/\beta,$$

$$\sigma = k\sqrt{1 - \beta^2}/\beta = k/\beta/\gamma, \quad \gamma = 1/\sqrt{1 - \beta^2},$$

$$\begin{aligned} I_\nu &\equiv I_\nu(a\sigma), & H_\nu &\equiv H_\nu^{(1)}(a\sigma), \\ I'_\nu &\equiv \left. \frac{dI_\nu(\xi)}{d\xi} \right|_{\xi=a\sigma}, & H'_\nu &\equiv \left. \frac{dH_\nu^{(1)}(\xi)}{d\xi} \right|_{\xi=a\sigma}, \end{aligned} \quad (8)$$

$$K_\nu \equiv K_\nu(a\sigma), \quad K'_\nu \equiv \left. \frac{dK_\nu(\xi)}{d\xi} \right|_{\xi=a\sigma}. \quad (9)$$

Note that the following recurrent formulas are useful for calculation of the derivatives:

$$\begin{aligned} I'_\nu &= I_{\nu+1} + \frac{\nu}{a\sigma} I_\nu, \\ K'_\nu &= -K_{\nu+1} + \frac{\nu}{a\sigma} K_\nu, \\ H'_\nu &= -H_{\nu+1} + \frac{\nu}{as} H_\nu, \end{aligned} \quad (10)$$

$$\tilde{A}_\nu^{(E2)} = \tilde{A}_\nu^{(E1)} \frac{I_\nu}{H_\nu} + \frac{K_\nu}{H_\nu}, \quad \tilde{A}_\nu^{(H2)} = \tilde{A}_\nu^{(H1)} \frac{I_\nu}{H_\nu}. \quad (11)$$

Phase $\Phi_i(r, z)$ is the phase of the CR inside the bulk of the target:

$$\Phi_i(r, z) = sr + \frac{kz}{\beta} - \frac{\pi}{4}.$$

Further the coordinates with primes denote the coordinates at the aperture. Taking into account that on the generatrix surface $r' = \xi' \sin(\alpha)$ and $z' = -\xi' \cos(\alpha)$, one can get this phase the generatrix surface as

$$\Phi_i(\xi') = s\xi' \sin \alpha - \frac{k}{\beta} \xi' \cos \alpha - \frac{\pi}{4} \quad (12)$$

Using (1) and (2) one can obtain the Fourier-transform of the field on the external surface of the aperture (surface

with coordinates $r' = \xi' \sin \alpha$ and $z' = -\xi' \cos \alpha$) in the following form:

$$\begin{aligned} H_{\varphi'} &\approx T_{\parallel} H_{\varphi'}^i(r', \varphi', z'), \\ E_{\xi'} &\approx H_{\varphi'} \cos \theta_t, \quad E_{\zeta'} \approx H_{\varphi'} \sin \theta_t; \end{aligned} \quad (13)$$

$$\begin{aligned} E_{\varphi'} &\approx T_{\perp} E_{\varphi'}^i(r', \varphi', z'), \\ H_{\xi'} &= -E_{\varphi'} \cos \theta_t, \quad E_{\zeta'} \approx -E_{\varphi'} \sin \theta_t. \end{aligned} \quad (14)$$

B. Aperture integrals

Now we should write the general Stratton-Chu formulas [13, 15, 17, 18] in the form which is convenient for further calculation in the case of considered target. We denote the cylindrical coordinates of the observation point \vec{R} as r, φ, z , and the coordinates of the point on the aperture as r', φ', z' :

$$r' = -z' \tan \alpha = \xi' \sin \alpha, \quad z' = -\xi' \cos \alpha.$$

The distance from the observation point to the point on the aperture is

$$\begin{aligned} \tilde{R} &= |\vec{R} - \vec{R}'| = \\ &= \sqrt{r^2 + \xi'^2 \sin^2 \alpha - 2r\xi' \sin \alpha \cos \tilde{\varphi} + (\xi' \cos \alpha + z)^2}, \end{aligned} \quad (15)$$

where $\tilde{\varphi} = \varphi' - \varphi$.

Remind that Stratton-Chu formulas include the series of differentiation operations over the Green function $G(\vec{R}) = \exp(ik\vec{R})/\vec{R}$. To simplify the formulas, we introduce the following small restriction: we assume that the distance from the observation point to the aperture is much more than the wavelength under consideration, that is, for all points on the aperture $k\tilde{R} \gg 1$. Then, we can differentiate the “fast” factor $\exp(ik\vec{R})$ only, and consider the “slow” factor $1/\tilde{R}$ as a constant.

The corresponding transformations of aperture integrals [13, 15, 17, 18] are cumbersome, but not very complicated. We give the final results for the electric field omitting all analytic calculations:

$$\vec{E}(\vec{R}) = \vec{E}^{(h)}(\vec{R}) + \vec{E}^{(e)}(\vec{R}),$$

$$E_r^{(h)}(\vec{R}) = \frac{ik}{4\pi} \int_{\Sigma} \left\{ -H_{\varphi'} \left[rr' \sin \alpha \sin^2 \tilde{\varphi} + (z' - z) (r' \cos \tilde{\varphi} - r) \cos \alpha + (z' - z)^2 \sin \alpha \cos \tilde{\varphi} \right] - \right. \\ \left. - H_{\xi'} \left[r'^2 - rr' \cos \tilde{\varphi} + (z' - z)^2 \right] \sin \tilde{\varphi} \right\} \frac{e^{ik\tilde{R}}}{\tilde{R}^3} d\Sigma' \quad (16)$$

$$E_{\varphi}^{(h)}(\vec{R}) \approx \frac{ik}{4\pi} \int_{\Sigma} \left\{ H_{\xi'} \left[(r^2 + r'^2 + (z' - z)^2) \cos \tilde{\varphi} - 2rr' (1 + \cos^2 \tilde{\varphi}) \right] - \right. \\ \left. - H_{\varphi'} \left[(r^2 - rr' \cos \tilde{\varphi} + (z' - z)^2) \sin \alpha + r' (z' - z) \cos \alpha \right] \sin \tilde{\varphi} \right\} \frac{e^{ik\tilde{R}}}{\tilde{R}^3} d\Sigma' \quad (17)$$

$$E_z^{(h)} = \frac{ik}{4\pi} \int_{\Sigma} \left\{ H_{\varphi'} \left[(r^2 + r'^2 - 2rr' \cos \tilde{\varphi}) \cos \alpha + (z' - z) (r' - r \cos \tilde{\varphi}) \sin \alpha \right] - H_{\xi'} r (z' - z) \sin \tilde{\varphi} \right\} \frac{e^{ik\tilde{R}}}{\tilde{R}^3} d\Sigma' \quad (18)$$

$$\begin{pmatrix} E_r^{(e)} \\ E_{\varphi}^{(e)} \\ E_z^{(e)} \end{pmatrix} = \frac{ik}{4\pi} \int_{\Sigma} \begin{pmatrix} E_{\xi'} (z' - z) \cos \tilde{\varphi} - E_{\varphi'} [r' \cos \alpha + (z' - z) \sin \alpha] \sin \tilde{\varphi} \\ E_{\xi'} (z' - z) \sin \tilde{\varphi} + E_{\varphi'} [\cos \alpha (r' \cos \tilde{\varphi} - r) + (z' - z) \sin \alpha \cos \tilde{\varphi}] \\ - E_{\xi'} (r' - r \cos \tilde{\varphi}) - E_{\varphi'} r \sin \alpha \sin \tilde{\varphi} \end{pmatrix} \frac{e^{ik\tilde{R}}}{\tilde{R}^2} d\Sigma', \quad (19)$$

where $\int_{\Sigma} d\Sigma' = \sin \alpha \int_{\xi_1}^{\xi_2} d\xi' \int_0^{2\pi} d\varphi' \xi'$. The integration limits ξ_1, ξ_2 are determined by the borders of the aperture:

$$\xi_1 = a / \sin \alpha, \quad \xi_2 = a / \sin \alpha + d. \quad (20)$$

C. Fraunhofer area

The formulas (16)–(19) can be simplified in the Fraunhofer (or far-field) area where the wave parameter is

large: $D = \frac{\lambda R}{\pi d^2} \gg 1$. In this region the wave is a quasi-plane transverse one, exactly speaking, a spherical wave with small curvature of the constant phase surface. Therefore it is convenient to use the spherical coordinates R, θ, φ . The nonzero components of the field in Fraunhofer area are equal approximately to the following:

$$E_{\theta} = \frac{ike^{ikR}}{4\pi R} \int_{\Sigma} \left\{ -H_{\varphi'} [(\cos \theta_t + \sin \alpha \cos \theta) \cos \tilde{\varphi} + \cos \alpha \sin \theta] + E_{\varphi'} (\sin \alpha + \cos \theta_t \cos \theta) \sin \tilde{\varphi} \right\} e^{ik\xi'\Phi} d\Sigma', \quad (21)$$

$$E_{\varphi} = \frac{ike^{ikR}}{4\pi R} \int_{\Sigma} \left\{ -H_{\varphi'} (\sin \alpha + \cos \theta_t \cos \theta) \sin \tilde{\varphi} - E_{\varphi'} [(\cos \theta_t + \sin \alpha \cos \theta) \cos \tilde{\varphi} + \cos \alpha \sin \theta] \right\} e^{ik\xi'\Phi} d\Sigma', \quad (22)$$

where

$$\Phi = \cos \alpha \cos \theta - \sin \alpha \sin \theta \cos \tilde{\varphi}.$$

The wave in far-field area is a transverse with respect to the vector \vec{R} ; correspondingly, E_R component is absent.

Note that, in the case $r_0 = 0$, the formulas (16) –

(19), as well as (21) and (22) are transformed into the corresponding formulas obtained in the paper [13].

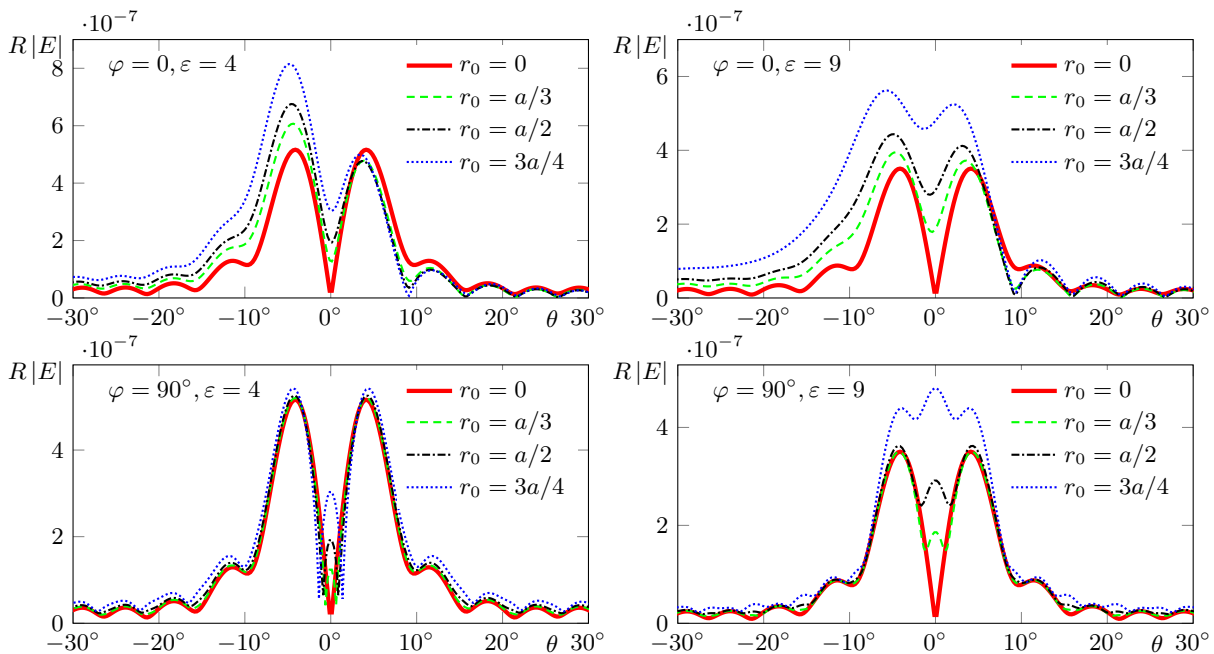


Figure 2. The angular distribution of the magnitude of the electric field Fourier-transform in the Fraunhofer area for the velocity $\beta = \beta_*$ corresponding to the case of “Cherenkov spotlight” (in units $V \cdot s$). Parameters: $a = c/\omega$, $d = 100c/\omega = 100/k$, $q = 1$ nC, $\mu = 1$, $\alpha = 20^\circ$; the permittivity ε , the charge shift r_0 , and the observation plane angle φ are indicated in the plots; $\beta = 0.6726$ for $\varepsilon = 4$ and $\beta = 0.5384$ for $\varepsilon = 9$. The negative values of θ correspond to value φ equal π plus the value φ indicated on the plot.

D. Results of computations

Here we demonstrate the results of computation of the field in Fraunhofer area obtained with use of formulas (21), (22). First of all, it is interesting to analyze the influence of the charge off-axis motion on the “Cherenkov spotlight” effect which was described in [13] for the case $r_0 = 0$.

Figure 2 shows the angle dependency of the field for different values of permittivity and for different shifts of the charge trajectory r_0 . It is assumed that the shift occurs in the side of positive values of x . The cross sections $\varphi = 0, \pi$ and $\varphi = \pi/2, 3\pi/2$ are shown. It is assumed that the velocity β corresponds to the case of “Cherenkov spotlight” effect for $r_0 = 0$ (this velocity is indicated as β_*). The vertical axis on the plots shows the value $R|E|$ which does not depend on the distance R in the Fraunhofer area. For convenience the negative values of θ in the figure correspond to positive ones for φ shifted on π .

Each plot contains four curves. For the bold red solid curve, the shift of the charge is zero (i.e. $r_0 = 0$); it illustrates the “Cherenkov spotlight” effect in symmetrical case. Other curves correspond to the cases when $r_0 \neq 0$. One can see that the spotlight effect is retained even when there is a large shift. Moreover, in the plane $\varphi = 0, \pi$, the radiation in the case $r_0 \neq 0$ is usually even more intense than in the case of $r_0 = 0$. Most significant increase of radiation occurs in the direction opposite to

the shift of the charge trajectory (that is, in the region of the negative angles φ). These effects can be explained by the fact that the excitation of Cherenkov radiation increases as the trajectory approaches the channel boundary. Another effect is that the field is not equal to zero on the structure axis in the case of $r_0 \neq 0$. Moreover, the field has a maximum on the symmetry axis in the cross section $\varphi = \pi/2, 3\pi/2$.

Besides the role of the trajectory offset, it is interesting to evaluate the effect of the velocity deviation from the “spotlight” velocity β_* . This effect is illustrated in Fig. 3, which shows the radiation amplitude at the velocity deviation of 10% from β_* . As you can see, this influence is very great. For $\beta = 1.1\beta_*$, the maximums shift and decrease essentially (green dashed lines), and for $\beta = 0.9\beta_*$, the spotlight effect practically disappears (black dash-dotted lines).

III. THE CASE OF “INVERTED” CONE

A. The field on the aperture

Let us now consider the problem with charge movement from the top of the cone to its base (Fig. 4). The radius of the cone base is $b + a$, and the cone angle is α . Accordingly, the length of the target along its axis is $l = b \cot \alpha$ and the distance from the top of the cone to its base is $l_0 = (a + b) \cot \alpha$. As earlier, we assume here

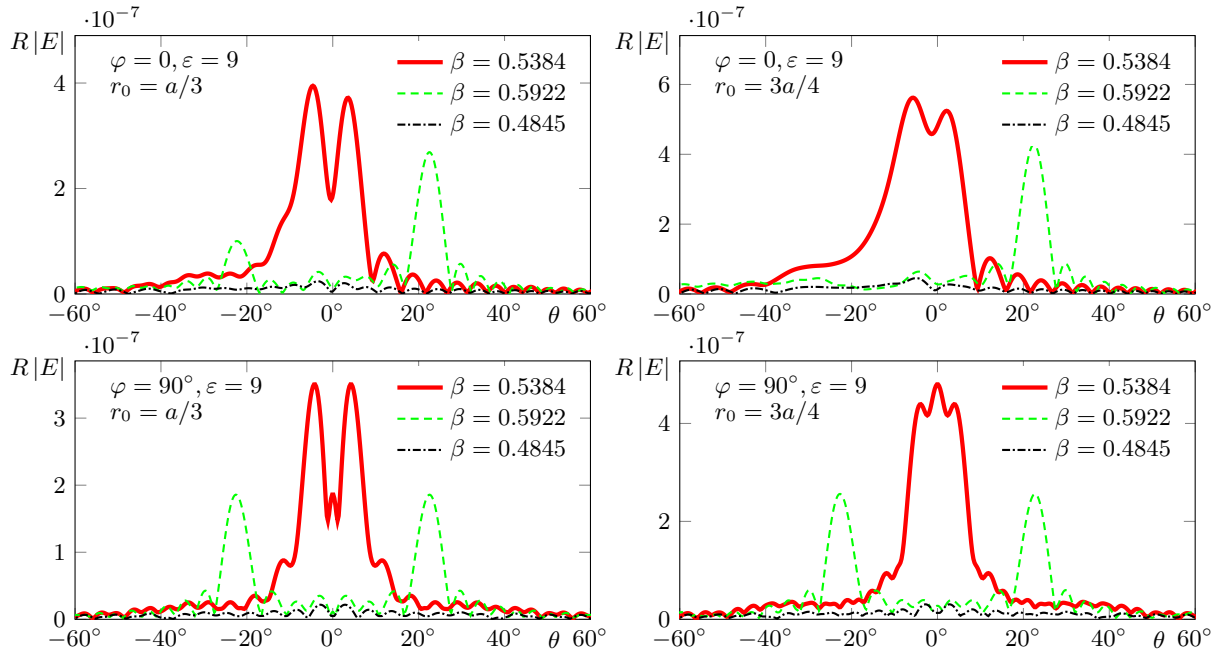


Figure 3. The same as in Fig. 2 for $\varepsilon = 9$ and different velocities: the red lines correspond to the velocity β_* (Cherenkov spotlight regime), the green dashed lines correspond to $\beta = 1.1\beta_*$, the black dashed-dotted line correspond to $\beta = 0.9\beta_*$.

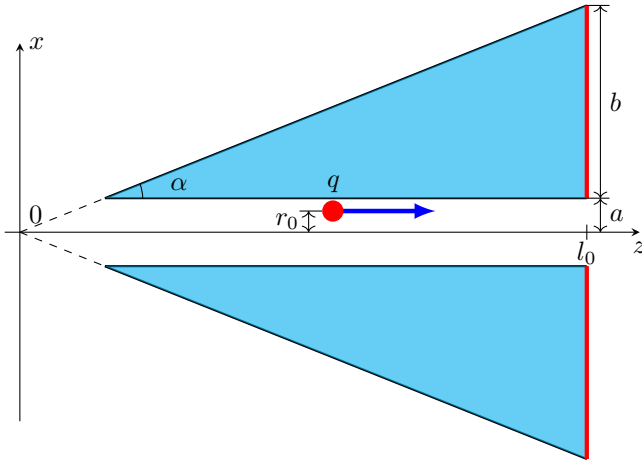


Figure 4. The “reversed” cone cross-section.

that the target size is much larger than the wavelength under consideration. Note that the axially symmetric case ($r_0 = 0$) has been analyzed by us in the paper [17].

The “etalon” problem for this situation is the same as in the Section 2 (this is the problem with the channel in the unbounded medium). Therefore the “initial” CR wave in the bulk of the target is determined by the formulas (3), (4).

We are mainly interested in the Cherenkov spotlight regime. As we have shown for the case when $r_0 = 0$ [], this effect can be realized with use of the wave which is once reflected from the cone generatrix [17] and then exits the target from its base surface. Therefore, the cone

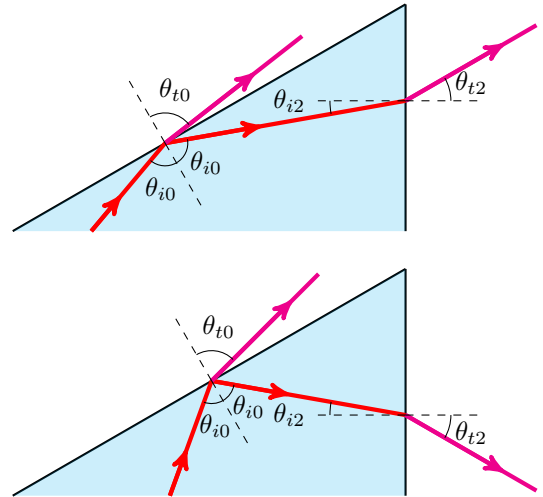


Figure 5. The path of the ray for the case $\theta_i > 0$ (top) and $\theta_i < 0$ (bottom).

base serves as the aperture in this case (solid red line in Fig. 4). We recall here the way of this wave (Fig. 5). This wave falls on the cone generatrix at the angle

$$\theta_{i0} = \pi/2 + \alpha - \theta_p \quad (\text{where } \theta_p = \arccos[1/(n\beta)]),$$

and reflects from it at the same angle $\theta_{r0} = \theta_{i0}$. Then this wave incidents the cone base at the angle

$$\theta_{i2} = \theta_{r0} - (\pi/2 - \alpha) = 2\alpha - \theta_p, \quad (23)$$

and refracts at the angle

$$\theta_{t2} = \arcsin(n \sin \theta_{i2}). \quad (24)$$

Cherenkov spotlight effect occurs if $\theta_{t2} = 0$. Thus, the wave experiences one reflection and one refraction in that case. For the wave with “parallel” polarization (\parallel) containing the components $E_{z\omega}$, $E_{r\omega}$ and $H_{\varphi\omega}$, the reflection coefficient (for the reflection at the cone generatrix) is

$$R_{\parallel 0} = \frac{\cos \theta_{i0} - \sqrt{\varepsilon} \cos \theta_{t0}}{\cos \theta_{i0} + \sqrt{\varepsilon} \cos \theta_{t0}}, \quad (25)$$

and the transmission coefficient (for the transmission at the cone base surface) is

$$T_{\parallel 2} = \frac{2 \cos \theta_{i2}}{\cos \theta_{i2} + \sqrt{\varepsilon} \cos \theta_{t2}}. \quad (26)$$

For the wave with “orthogonal” polarization (\perp) containing the components $H_{z\omega}$, $H_{r\omega}$ and $E_{\varphi\omega}$, corresponding coefficients are

$$R_{\perp 0} = \frac{\sqrt{\varepsilon} \cos \theta_{i0} - \cos \theta_{t0}}{\sqrt{\varepsilon} \cos \theta_{i0} + \cos \theta_{t0}}. \quad (27)$$

$$T_{\perp 2} = \frac{2\sqrt{\varepsilon} \cos \theta_{i1}}{\sqrt{\varepsilon} \cos \theta_{i1} + \cos \theta_{t1}}. \quad (28)$$

Omitting intermediate transformations, we now present the result for the Fourier transforms of the field components at the aperture at the point with cylindrical coordinates r' , φ' , $z' = l_0 + 0$:

$$\begin{aligned} H_{\varphi'}|_{z'=l_0+0} &\approx R_{\parallel 0} T_{\parallel 2} H_{\varphi'}^i(r', \varphi', l_0), \\ E_{r'} &\approx H_{\varphi'} \cos \theta_{t2}, \\ E_{z'} &\approx -H_{\varphi'} \sin \theta_{t2}; \end{aligned} \quad (29)$$

$$E_r^{(h)} = -\frac{ik}{4\pi} \int_{\Sigma} \left[H_{r'} \sin \tilde{\varphi} (r'^2 - rr' \cos \tilde{\varphi} + \tilde{z}^2) + H_{\varphi'} (rr' \sin^2 \tilde{\varphi} + \tilde{z}^2 \cos \tilde{\varphi}) \right] \frac{e^{ik\tilde{R}}}{\tilde{R}^3} d\Sigma', \quad (32)$$

$$E_r^{(h)} = \frac{ik}{4\pi} \int_{\Sigma} \left\{ H_{r'} \left[(r^2 + r'^2 + \tilde{z}^2) \cos \tilde{\varphi} - rr' (1 + \cos^2 \tilde{\varphi}) \right] - H_{\varphi'} \sin \tilde{\varphi} [r^2 - rr' \cos \tilde{\varphi} + \tilde{z}^2] \right\} \frac{e^{ik\tilde{R}}}{\tilde{R}^3} d\Sigma', \quad (33)$$

$$E_r^{(h)} = -\frac{ik\tilde{z}}{4\pi} \int_{\Sigma} [H_{\varphi'} (r' - r \cos \tilde{\varphi}) - H_{r'} r \sin \tilde{\varphi}] \frac{e^{ik\tilde{R}}}{\tilde{R}^3} d\Sigma', \quad (34)$$

$$\begin{Bmatrix} E_r^{(e)} \\ E_{\varphi}^{(e)} \\ E_z^{(e)} \end{Bmatrix} = -\frac{ik}{4\pi} \int_{\Sigma} \begin{Bmatrix} (E_{r'} \cos \tilde{\varphi} - E_{\varphi'} \sin \tilde{\varphi}) \tilde{z} \\ (E_{r'} \sin \tilde{\varphi} + E_{\varphi'} \cos \tilde{\varphi}) \tilde{z} \\ E_{r'} (r' - r \cos \tilde{\varphi}) + E_{\varphi'} r \sin \tilde{\varphi} \end{Bmatrix} \frac{e^{ik\tilde{R}}}{\tilde{R}^2} d\Sigma', \quad (35)$$

where $\int_{\Sigma} d\Sigma' = \int_a^{a+b} r' dr' \int_0^{2\pi} d\varphi'$.

$$\begin{aligned} E_{\varphi'}|_{z'=l_0+0} &\approx R_{\perp 0} T_{\perp 2} E_{\varphi'}^i(r', \varphi', l_0), \\ H_{r'} &\approx -E_{\varphi'} \cos \theta_{t2}, \\ H_{z'} &\approx E_{\varphi'} \sin \theta_{t2}. \end{aligned} \quad (30)$$

The expressions for $H_{\varphi'}^i$ and $E_{\varphi'}^i$ are formally coincide with (3), (4) however the formula for Φ_i is different. Calculation give the following result:

$$\begin{aligned} \Phi_i(r', z') &= kn (r' \sin \theta_{i2} + z' \cos \theta_{i2}) - \pi/4 = \\ &= kr' \sin \theta_{t2} + knz' \cos \theta_{i2} - \pi/4, \end{aligned} \quad (31)$$

B. Aperture integrals

Let us write the general Stratton-Chu formulas [13, 15, 17, 18] in the form which is convenient for further calculation. Remind that we denote the cylindrical coordinates of the observation point \vec{R} as r, φ, z , and the coordinates of the point on the aperture \vec{R}' as r', φ', z' . The distance from the observation point to the point on the aperture is $\tilde{R} = \sqrt{r^2 + r'^2 - 2rr' \cos \tilde{\varphi} + \tilde{z}^2}$, where $\tilde{\varphi} = \varphi' - \varphi$, $\tilde{z} = z - l_0$.

As in the previous section, we assume, that the distance from the observation point to any point on the aperture is much more than the wavelength under consideration: $k\tilde{R} \gg 1$. It allows to differentiate only the “fast” factor $\exp(ik\tilde{R})$ in the Green function considering the “slow” factor $1/\tilde{R}$ as a constant.

We give the final result for the electric field Fourier transform omitting all transformations:

$$\vec{E}(\vec{R}) = \vec{E}^{(h)}(\vec{R}) + \vec{E}^{(e)}(\vec{R}),$$

C. Fraunhofer area

The formulas (32)–(35) can be simplified in the Fraunhofer (or far-field) area where the wave parameter is large: $D = \lambda R/(\pi d^2) \gg 1$. In this region, the wave is a spherical transverse wave with small curvature of constant phase surface. Using the spherical coordinates R, θ, φ one can write the nonzero components of the field in Fraunhofer area in the following form:

$$E_\theta = \frac{ik \exp(ikR - ikl_0 \cos \theta)}{4\pi R} \int_{\Sigma} [E_{\varphi'} (1 + \cos \theta_t \cos \theta) \sin \tilde{\varphi} - H_{\varphi'} (\cos \theta_t + \cos \theta) \cos \tilde{\varphi}] e^{-ikr' \sin \theta \cos \tilde{\varphi}} d\Sigma', \quad (36)$$

$$E_\varphi = \frac{ik \exp(ikR - ikl_0 \cos \theta)}{4\pi R} \int_{\Sigma} [-E_{\varphi'} (\cos \theta_t + \cos \theta) \cos \tilde{\varphi} - H'_{\varphi'} (1 + \cos \theta_t \cos \theta) \sin \tilde{\varphi}] e^{-ikr' \sin \theta \cos \tilde{\varphi}} d\Sigma'. \quad (37)$$

If $r_0 = 0$ then the formulas (32) – (35), as well as (36) and (37) are transformed into the corresponding formulas obtained in the paper [17].

D. Results of computations

The results of computation of the field obtaining by the formulas (36), (37) are shown in Fig. 6, 7. First of all, we demonstrate the influence of the charge off-axis motion on the “Cherenkov spotlight” effect which was described in [17] for the case $r_0 = 0$.

Figure 6 shows the angular dependency of the field for different values of permittivity and for different shifts of the charge trajectory r_0 . It is assumed that the shift occurs in the side of positive values of x . The cross sections $\varphi = 0, \pi$ and $\varphi = \pi/2, 3\pi/2$ are shown. It is assumed that the velocity β corresponds to the case of “Cherenkov spotlight” effect for $r_0 = 0$ (this velocity is indicated as β_*). The vertical axis on the plots shows the value of $R|E|$ which does not depend on the distance R in the Fraunhofer area. For convenience the negative values of θ in the figure correspond to positive ones for φ shifted on π . For the bold red solid curves, the shift of the charge is zero ($r_0 = 0$); it illustrates the “Cherenkov spotlight” effect in symmetrical case. Other curves correspond to the cases when $r_0 \neq 0$.

The main conclusions here are the same as in the case of the straight cone, namely:

- The spotlight effect is retained even when there is the large shift of the charge trajectory; moreover, in the plane $\varphi = 0, \pi$, the radiation in the case $r_0 \neq 0$ is usually even more intense than in the case of $r_0 = 0$;
- Most significant increase of radiation occurs in the direction opposite to the shift of the charge trajectory;
- The field is not equal to zero on the structure axis in the case of $r_0 \neq 0$.

The influence of the velocity deviation on the spotlight regime is illustrated in Fig. 7 which shows the field value at the velocity differing in 10% from the “spotlight velocity” β_* . It is interesting that this influence is much

less than in the case of the straight cone (compare Fig. 7 and Fig. 3). The spotlight effect is fully retained when the speed is changed by 10%. Moreover, under certain conditions, the radiation is obtained even more than with $\beta = \beta_*$.

Thus, the inverted cone offers significant advantages for realizing the spotlight effect over the straight cone. These schemes are equally insensitive to variations in the displacement of the trajectory from the axis. However the radiation from the inverted cone is much more stable with respect to variations in the charge velocity. Earlier, one more important advantage of the inverted cone was also noted [17]: with such a scheme, it is always possible to select the cone parameters, which would make it possible to realize the spotlight effect (including the case of ultrarelativistic charge). For the straight cone, there are significant limits on the charge speed at which the spotlight effect is achievable.

IV. CONCLUSION

We investigated Cherenkov radiation generated by charge moving in channel in the dielectric cone. Unlike previous works, a shift of the charge trajectory from the symmetry axis was taken into account. We applied the aperture method which was developed by us earlier. The most attention was given to phenomenon of “Cherenkov spotlight” which was reported earlier for axially symmetrical problems. This effect allows essential enhancement of Cherenkov radiation intensity in the far-field region by proper selection of the target’s parameters.

We analyzed the influence of the shift of the charge trajectory from the symmetry axis on the spotlight regime, as well as the effect of the charge velocity variation. The main conclusions consist in the following. The spotlight effect is retained even for large displacement of trajectory from the symmetry axis both in case of the straight cone and in case of the inverted cone. The radiation can be even more than for the central motion of charge. The most significant increase of radiation occurs in the direc-

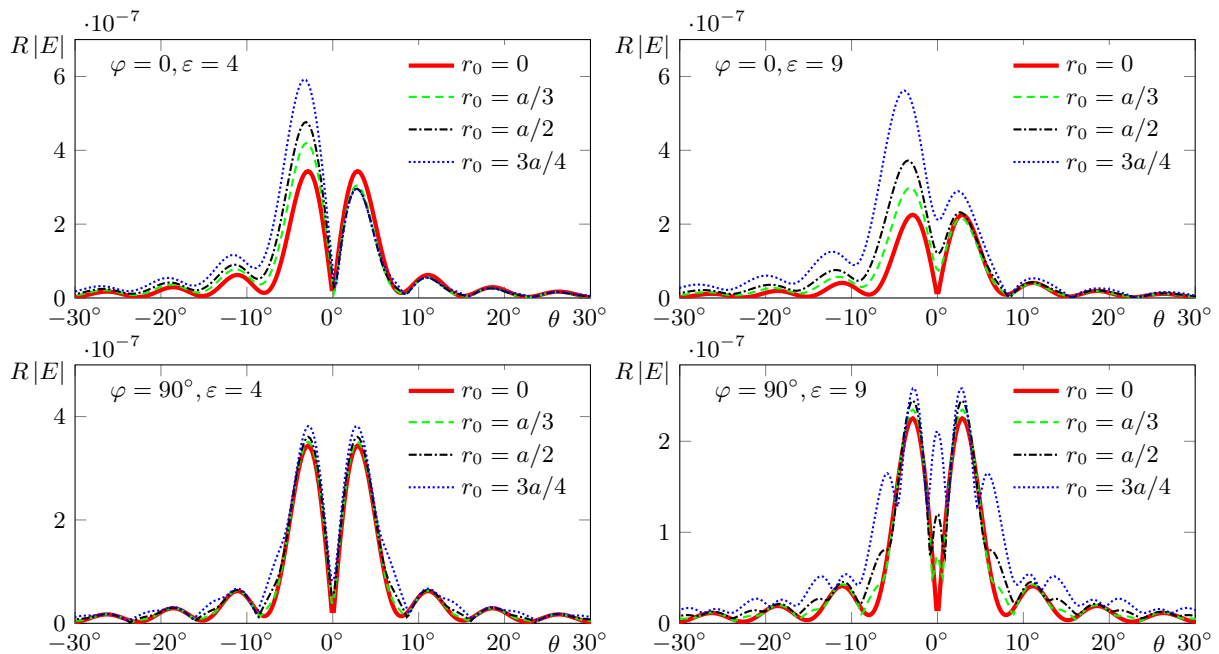


Figure 6. The angular distribution of the magnitude of the electric field Fourier-transform in the Fraunhofer area for the velocity $\beta = \beta_*$ corresponding to the case of “Cherenkov spotlight” (in units $V \cdot s$). Parameters: $a = c/\omega$, $b = 50c/\omega = 50/k$, $q = 1$ nC, $\mu = 1$, $\alpha = 20^\circ$; the charge shift r_0 , the permittivity ε , and the observation angle φ are indicated in the plots; $\beta = 0.6527$ for $\varepsilon = 4$ and $\beta = 0.4351$ for $\varepsilon = 9$. The negative values of θ correspond to value φ equal π plus the value φ indicated on the plot.

tion opposite to the shift of the charge trajectory. However the radiation from the inverted cone is much more stable with respect to variations in the charge velocity. It is important as well that the inverted cone allows reaching the spotlight phenomenon for any speed of charge (due to selection of the cone parameters), while, for the straight cone, there are significant limits on the charge

velocity which allow reaching the spotlight regime.

V. ACKNOWLEDGEMENTS

This research was supported by the Russian Science Foundation, Grant No. 18-72-10137.

-
- [1] V. P. Zrelov, *Vavilov-Cherenkov Radiation in High-Energy Physics* (Israel Program for Scientific Translations, Jerusalem, 1970).
 - [2] A. P. Potylitsyn, Y. A. Popov, L. G. Sukhikh, G. A. Naumenko, and M. V. Shevelev, *Journal of Physics: Conference Series* **236**, 012025 (2010).
 - [3] M. I. Ryazanov, M. N. Strikhanov, and A. A. Tishchenko, *Journal of Experimental and Theoretical Physics* **99**, 311 (2004).
 - [4] D. V. Karlovets, *Journal of Experimental and Theoretical Physics* **113**, 27 (2011).
 - [5] M. Shevelev, A. Konkov, and A. Aryshev, *Phys. Rev. A* **92**, 053851 (2015).
 - [6] E. S. Belonogaya, A. V. Tyukhtin, and S. N. Galyamin, *Phys. Rev. E* **87**, 043201 (2013).
 - [7] E. S. Belonogaya, S. N. Galyamin, and A. V. Tyukhtin, *J. Opt. Soc. Am. B* **32**, 649 (2015).
 - [8] S. N. Galyamin and A. V. Tyukhtin, *Phys. Rev. Lett.* **113**, 064802 (2014).
 - [9] S. N. Galyamin, A. V. Tyukhtin, S. Antipov, and S. S. Baturin, *Opt. Express* **22**, 8902 (2014).
 - [10] S. N. Galyamin, A. V. Tyukhtin, S. Antipov, and S. S. Baturin, *Opt. Express* **22**, 8902 (2014).
 - [11] S. N. Galyamin and A. V. Tyukhtin, *Nuclear Instruments and Methods in Physics Research Section B: Beam Interactions with Materials and Atoms* **402**, 185 (2017).
 - [12] A. Tyukhtin, V. Vorobev, E. Belonogaya, and S. Galyamin, *Journal of Instrumentation* **13**, C02033 (2018).
 - [13] A. V. Tyukhtin, S. N. Galyamin, and V. V. Vorobev, *Phys. Rev. A* **99**, 023810 (2019).
 - [14] A. V. Tyukhtin, V. V. Vorobev, S. N. Galyamin, and E. S. Belonogaya, *Phys. Rev. Accel. Beams* **22**, 012802 (2019).
 - [15] S. N. Galyamin, V. V. Vorobev, and A. V. Tyukhtin, *Phys. Rev. Accel. Beams* **22**, 083001 (2019).
 - [16] S. N. Galyamin, V. V. Vorobev, and A. V. Tyukhtin, *Phys. Rev. Accel. Beams* **22**, 109901 (2019).

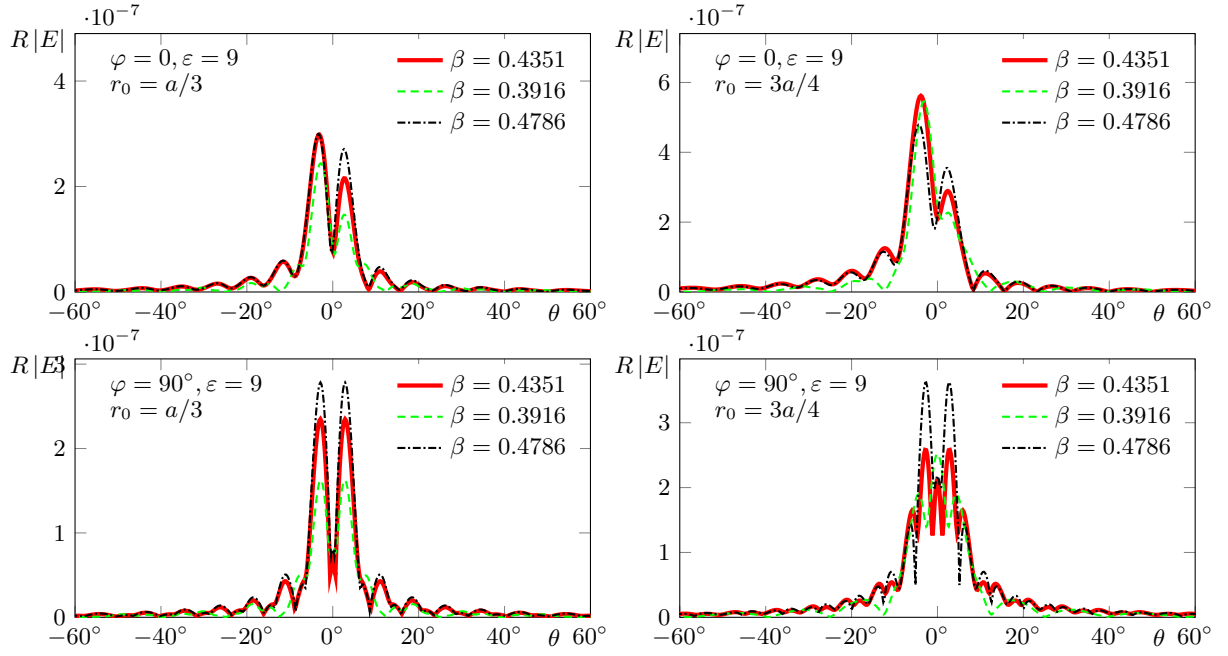


Figure 7. The same as in Fig. 6 for $\varepsilon = 9$ and different velocities: the red lines correspond to the velocity β_* (Cherenkov spotlight regime), the green dashed lines correspond to $\beta = 1.1\beta_*$, the black dashed-dotted line correspond to $\beta = 0.9\beta_*$.

- [17] A. V. Tyukhtin, S. N. Galyamin, V. V. Vorobev, and A. A. Grigoreva, *Phys. Rev. A* **102**, 053514 (2020).
- [18] A. V. Tyukhtin, S. N. Galyamin, and V. V. Vorobev, *J. Opt. Soc. Am. B* **38**, 711 (2021).
- [19] J. H. McLeod, *J. Opt. Soc. Am.* **44**, 592 (1954).
- [20] R. M. Herman and T. A. Wiggins, *J. Opt. Soc. Am. A* **8**, 932 (1991).
- [21] Y. Y. Choporova, B. A. Knyazev, G. N. Kulipanov, V. S. Pavelyev, M. A. Scheglov, N. A. Vinokurov, B. O. Volodkin, and V. N. Zhabin, *Phys. Rev. A* **96**, 023846 (2017).
- [22] W. D. Kimura, H. M. Milchberg, P. Muggli, X. Li, and W. B. Mori, *Phys. Rev. ST Accel. Beams* **14**, 041301 (2011).
- [23] G. Hatakoshi, M. Kawachi, K. Terashima, Y. Uematsu, A. Amano, and K. Ueda, *Opt. Lett.* **15**, 1336 (1990).
- [24] A. Fradin, *Microwave Antennas* (Pergamon, New York, 1961).
- [25] B. M. Bolotovskii, *Sov. Phys. Usp.* **4**, 781 (1962).
- [26] A. P. Prudnikov, Y. A. Brychkov, and O. I. Marichev, *Integrals and Series: Elementary Functions* (Gordon & Breach Sci., New York, 1986).
- [27] M. Abramowitz and I. A. Stegun, *Handbook of Mathematical Functions with Formulas, Graphs, and Mathematical Tables* (Dover, New York, 1964).
- [28] V. L. Ginzburg and V. N. Tsytovich, *Transition Radiation and Transition Scattering* (Higler, London, 1990).
- [29] A. P. Prudnikov, Y. A. Brychkov, and O. I. Marichev, *Integrals and Series, Vol. 1, Elementary Functions* (Gordon & Breach Sci. Publ., New York, 1986).
- [30] M. Abramowitz and I. A. Stegun, eds., *Handbook of Mathematical Functions: with Formulas, Graphs, and Mathematical Tables* (Dover Publications, New York, 1972).